

Bottom-up Higher-Resolution Networks for Multi-Person Pose Estimation

Bowen Cheng¹, Bin Xiao^{2*}, Jingdong Wang³, Honghui Shi^{1,4}, Thomas S. Huang¹, Lei Zhang³

¹UIUC, ²ByteDance, ³Microsoft, ⁴University of Oregon

Abstract

In this paper, we are interested in bottom-up multi-person human pose estimation. A typical bottom-up pipeline consists of two main steps: heatmap prediction and keypoint grouping. We mainly focus on the first step for improving heatmap prediction accuracy. We propose Higher-Resolution Network (HigherHRNet), which is a simple extension of the High-Resolution Network (HRNet). HigherHRNet generates higher-resolution feature maps by deconvolving the high-resolution feature maps outputted by HRNet, which are spatially more accurate for small and medium persons. Then, we build high-quality multi-level features and perform multi-scale pose prediction. The extra computation overhead is marginal and negligible in comparison to existing bottom-up methods that rely on multi-scale image pyramids or large input image size to generate accurate pose heatmaps. HigherHRNet surpasses all existing bottom-up methods on the COCO dataset without using multi-scale test. The code and models will be released.

1. Introduction

2D human pose estimation aims at localizing human anatomical keypoints (e.g., elbow, wrist, etc.) or parts. As a fundamental technique to human behavior understanding, it has received increasing attention in recent years.

Current human pose estimation methods can be categorized into *top-down* methods and *bottom-up* methods. Top-down methods [25, 8, 11, 32, 29, 30, 11] take a dependency on person detector to detect person instances each with a bounding box and then reduce the problem to a simpler task of single person pose estimation. As top-down methods can normalize all the persons to approximately the same scale by cropping and resizing the detected person bounding boxes, they are generally less sensitive to the scale variance of persons. Thus, most state-of-the-art performances on various multi-person human pose estimation benchmarks are achieved by top-down methods. However, as such meth-

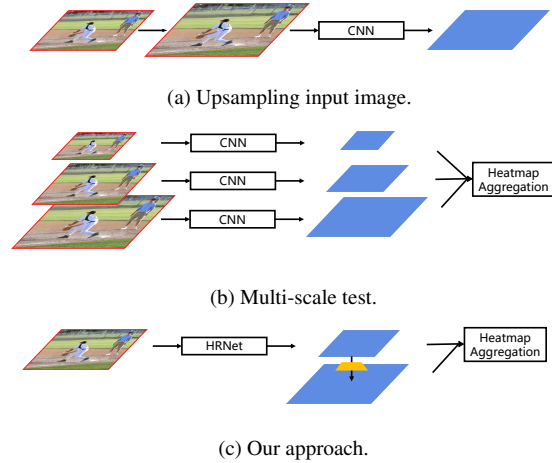


Figure 1. (a) Generating higher resolution and spatially more accurate heatmaps by upsampling image. Recent work PersonLab [24] relies on enlarging input image size to generate high quality feature maps. (b) Using multi-scale test for heatmap prediction [24, 22]. (c) Using High-Resolution Net (HRNet) as backbone to output high quality feature maps, followed by a deconvolution module to generate higher resolution and spatially more accurate heatmaps.

ods rely on a separate person detector and need to estimate pose for every person individually, they are normally computationally intensive and not truly end-to-end systems. By contrast, bottom-up methods [2, 22, 24] start by localizing identity-free keypoints for all the persons in an input image through predicting heatmaps of different anatomical keypoints, followed by grouping them into person instances. This strategy effectively makes bottom-up methods faster and more capable of achieving real-time pose estimation. However, there still exists a large gap between the performances of bottom-up and top-down methods.

Newell *et al.* [22] find that in bottom-up methods, person grouping is easier than keypoint detection and grouping can already generate reliable results by associative embedding [22]. The main problem of bottom-up methods lies in inaccurate heatmap prediction. In most cases, bottom-up methods are good at localizing keypoints precisely for large

*This work was done while Bin Xiao was at Microsoft.

persons while inaccurate for smaller persons. We hypothesize the inferior in keypoint prediction for smaller persons is caused by insufficient feature map resolution. As feature maps with different resolutions are generally sensitive to different scales of objects, this also makes training bottom-up networks harder. To address these problems, most existing bottom-up methods either resort to multi-scale image pyramids [2, 22, 24] (Figure 1 (a)) or larger input image size [24] (Figure 1 (b)) to generate more accurate heatmaps during testing time. However, both testing methods introduce more computational cost which contradicts to the original intention of making bottom-up methods more efficient. To solve these problems, we target at generating spatially more accurate and scale-aware heatmaps for bottom-up keypoint prediction in a natural and simple way without sacrificing computational cost.

In this paper, we propose a Higher-Resolution Network (HigherHRNet) for generating spatially more accurate and scale-aware heatmaps. HigherHRNet is an extension of High-Resolution Network (HRNet) [29], which was initially developed for top-down human pose estimation, by simply adding one or more deconvolution modules. Furthermore, HigherHRNet is naturally equipped with high quality multi-resolution heatmaps that can be used for heatmap aggregation with small computation overhead (Figure 1 (c)).

Our goal is to solve multi-person pose estimation in a simple and elegant way. We do not use multi-scale test to boost performance. We demonstrate superior keypoint detection performance on the COCO keypoint detection dataset [20]. Specifically, HigherHRNet achieves AP of 70.4 on COCO2017 test-dev with *single scale test*, outperforming all existing bottom-up methods by a large margin.

To summarize our main contributions:

- We propose a Higher Resolution Network (HigherHRNet) by adding an efficient deconvolution module on the High Resolution Network (HRNet) [29] with small computation overhead.
- We propose a Multi-Resolution Supervision in training stage and a Heatmap Aggregation strategy for inference to let HigherHRNet predict scale-aware heatmaps.
- We demonstrate the effectiveness of our HigherHRNet on the challenging COCO dataset. Our model outperforms all other bottom-up methods.

2. Related works

Top-down methods. Top-down methods [32, 29, 25, 11, 13, 10, 8, 23] detect a single person keypoints within a person bounding box. The person bounding boxes are usually generated by an object detector [27, 19, 9]. Mask R-CNN [11] directly adds a keypoint detection branch on

Faster R-CNN [27] and reuses features after ROIpooling. G-RMI [25] and the following methods further break top-down methods into two steps and use separate models for person detection and pose estimation.

Bottom-up methods. Bottom-up methods [26, 14, 15, 2, 22] detect identity-free body joints for all the persons in an image and then group them into individuals. OpenPose [2] uses a two-branch multi-stage network with one branch for heatmap prediction and one branch for grouping. OpenPose uses a grouping method named part affinity field which learns a 2D vector field linking two keypoints. Grouping is done by calculating line integral between two keypoints and group the pair with the largest integral. Newell *et al.* [22] use stacked hourglass network [23] for both heatmap prediction and grouping. Grouping is done by a method named associate embedding, which assigns each keypoint with a “tag” (a vector representation) and groups keypoints based on the l_2 distance between tag vectors. PersonLab [24] uses dilated ResNet [12] and groups keypoints by directly learning a 2D offset field for each pair of keypoints.

High resolution feature maps. There are mainly 4 methods to generate high resolution feature maps. (1) Encoder-decoder [23, 11, 8, 28, 1, 18, 31] captures the context information in the encoder path and recover high resolution features in the decoder path. The decoder usually contains a sequence of bilinear upsample operations with skip connections from encoder features with the same resolution. (2) Dilated convolution [34, 5, 4, 6, 7, 3, 21, 33] (*a.k.a.* “atrous” convolution) is used to remove several stride convolutions/max poolings to preserve feature map resolution. Dilated convolution prevents losing spatial information but introduces more computational cost. (3) Deconvolution (transposed convolution) [32] is used in sequence at the end of a network to efficiently increase feature map resolution. SimpleBaseline [32] demonstrates that deconvolution can generate high quality feature maps for heatmap prediction. (4) Recently, a High-Resolution Network (HRNet) [29] is proposed as an efficient way to keep a high resolution pass throughout the network. HRNet [29] consists of multiple branches with different resolutions. Lower resolution branches capture contextual information and higher resolution branches preserve spatial information. With multi-scale fusions between branches, HRNet [29] can generate high resolution feature maps with rich semantic.

Our work is inspired by SimpleBaseline [32] and HRNet [29]. We adopt HRNet [29] as our base network to generate high-quality feature maps. And we add a deconvolution module to generate higher resolution feature maps to predict heatmaps. The resulting model is named “Higher-Resolution Network” (HigherHRNet). As both HRNet [29] and deconvolution are efficient, HigherHRNet is an effi-

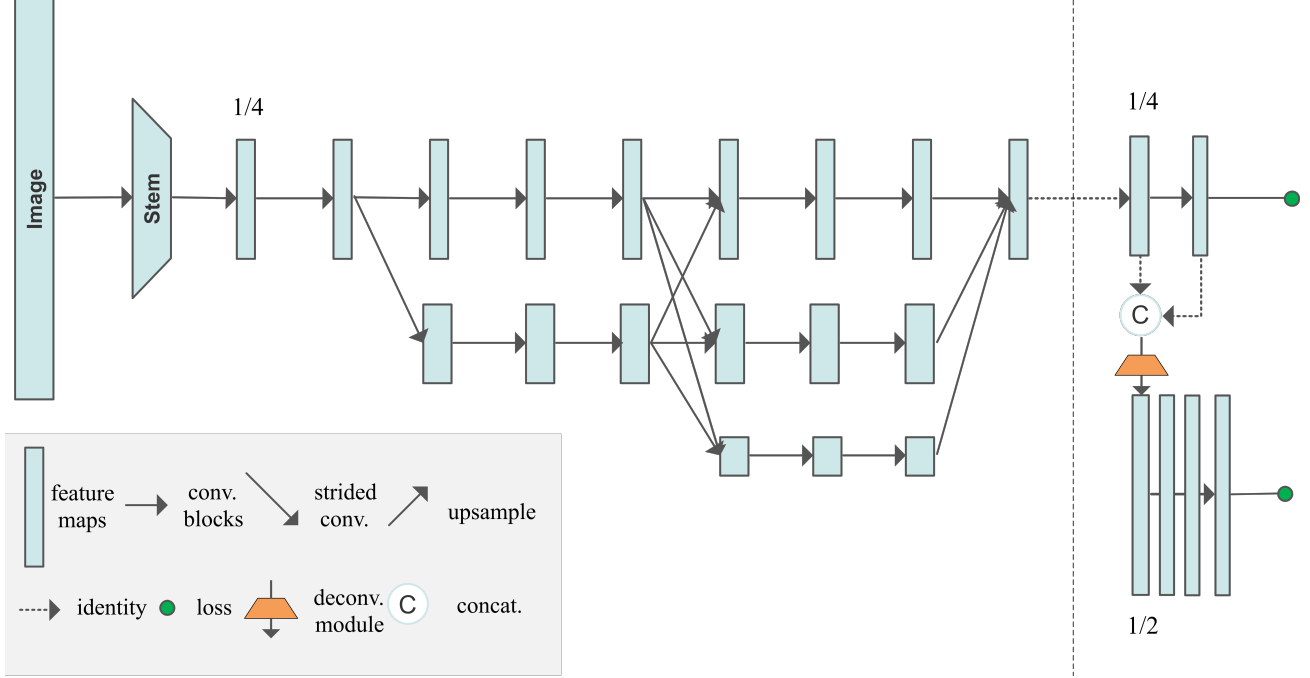


Figure 2. An illustration of HigherHRNet. The network uses HRNet [29] as backbone, followed by one or more deconvolution modules to generate multi-resolution and high-resolution heatmaps. Multi-resolution supervision is used for training. More details are given in Section 3.

cient model for generating higher resolution feature maps for heatmap prediction.

3. Higher-Resolution Network

In this section, we introduce our proposed Higher-Resolution Network (HigherHRNet). Figure 2 illustrates the overall architecture of our method. We will firstly give a brief overview on the proposed HigherHRNet and then describe its components in details.

3.1. HigherHRNet

HRNet. HigherHRNet uses HRNet [29] (shown in Figure 2) as backbone. HRNet [29] starts with a high-resolution branch in the first stage. In every following stage, a new branch is added to current branches in parallel with resolution $\frac{1}{2}$ of the lowest resolution in current branches. As the network has more stages, it will have more parallel branches with different resolutions and resolutions from previous stage are all preserved in later stages. An example network structure, containing 3 parallel branches, is illustrated in Figure 2.

We instantiate the backbone using a similar manner as HRNet [29]. The network starts from a stem that consists of two strided 3×3 convolutions decreasing the resolution to $1/4$. The 1st stage contains 4 residual units where each unit is formed by a bottleneck with width 64, followed by one 3×3 convolution reducing the width of feature maps to C .

The 2nd, 3rd, 4th stages contain 1, 4, and 3 multi-resolution blocks, respectively. The widths (number of channels) of the convolutions of the four resolutions are C , $2C$, $4C$, and $8C$, respectively. Each branch in the multi-resolution group convolution has 4 residual units and each unit has two 3×3 convolutions in each resolution. In all our experiments, we set C to 32.

HRNet [29] was originally designed for top-down pose estimation. In this work, we adopt HRNet [29] to a bottom-up method by adding a 1×1 convolution to predict heatmaps and tagmaps similar to [22]. We only use the highest resolution ($\frac{1}{4}$ of the input image) feature maps for prediction. Following [22], we use scalar tag for each keypoint.

HigherHRNet. Most existing human pose estimation methods predict Gaussian-smoothed heatmaps by preparing the ground truth headmaps with an unnormalized Gaussian kernel applied to each keypoint location. Adding this Gaussian kernel helps training networks as CNNs tend to output spatially smooth responses as a nature of convolution operations. However, applying a Gaussian kernel also introduces confusion in precise localization of keypoints. A trivial solution to reduce this confusion is to reduce the *std* of the Gaussian kernel. However, we empirically find that it makes optimization harder and leads to even worse results.

Instead of reducing *std*, we solve this problem by predicting heatmaps at higher resolution with *std* unchanged

at different resolutions. Bottom-up methods usually predict heatmaps at resolution $\frac{1}{4}$ of the input image. Yet we find this resolution is not high enough for predicting accurate heatmaps. Inspired by [32], which shows that deconvolution can be used to effectively generate high quality and high resolution feature maps, we build HigherHRNet on top of the highest resolution feature maps in HRNet as shown in Figure 2 by adding a deconvolution module as discussed in Section 3.3.

The deconvolution module takes as input both features and predicted heatmaps from HRNet and generates new feature maps that are 2 times larger in resolution than the input feature maps. A feature pyramid with two resolutions is thus generated by the deconvolution module together with the feature maps from HRNet. The deconvolution module also predicts heatmaps by adding an extra 1×1 convolution. We follow Section 3.4 to train heatmap predictors at different resolutions and use a heatmap aggregation strategy as described in (Section 3.5) for inference.

More deconvolution modules can be added if larger resolution is desired. We find the number of deconvolution modules is dependent on the distribution of person scales of the dataset. Generally speaking, a dataset containing smaller persons requires larger resolution feature maps for prediction and vice versa. In experiments, we find adding a single deconvolution module achieves the best performance on the COCO dataset.

3.2. Grouping.

Recent works [22, 17] have shown that grouping can be solved with high accuracy by a simple method using associative embedding [22]. As an evidence, experimental results in [22] show that using the ground truth detections with the predicted tags improves AP from 59.2 to 94.0 on a held-out set of 500 training images of the COCO keypoint detection dataset [20]. We follow [22] to use associative embedding for keypoint grouping. The grouping process clusters identity-free keypoints into individuals by grouping keypoints whose tags have small l_2 distance.

3.3. Deconvolution Module

We propose a simple deconvolution module for generating high quality feature maps whose resolution is two times higher than the input feature maps. Following [32], we use a 4×4 deconvolution (*a.k.a.* transposed convolution) followed by BatchNorm and ReLU to learn to upsample the input feature maps. Optionally, we could further add several Basic Residual Blocks [12] after deconvolution to refine the upsampled feature maps. We add 4 Residual Blocks in HigherHRNet.

Different from [32], the input to our deconvolution module is the concatenation of the feature maps and the predicted heatmaps from either HRNet or previous deconvolution modules.

And the output feature maps of each deconvolution module are also used to predict heatmaps in a multi-scale fashion.

3.4. Multi-Resolution Supervision

Unlike other bottom-up methods [22, 24, 2] that only apply supervision to the largest resolution heatmaps, we introduce a multi-resolution supervision during training. We transform ground truth keypoint locations to locations on the heatmaps of all resolutions to generate ground truth heatmaps with different resolutions. Then we apply a Gaussian kernel with the same standard deviation (we use $std = 2$ by default) to all these ground truth heatmaps.

At each prediction scale in HigherHRNet, we calculate the mean squared error between the predicted heatmaps of that scale and its associated ground truth heatmaps. The final loss for heatmaps is the sum of mean squared errors for all resolutions.

Tagmaps are trained differently from heatmaps in HigherHRNet. We only predict tagmaps at the lowest resolution, instead of using all resolutions. This is because learning tagmaps requires global reasoning and it is more suitable to predict tagmaps in lower resolution. Empirically, we also find higher resolutions do not learn to predict tagmaps well and even do not converge. Thus, we follow [22] to train the tagmaps on feature maps at $\frac{1}{4}$ resolution of input image.

3.5. Heatmap Aggregation for Inference

We propose a heatmap aggregation strategy during inference. We use bilinear interpolation to upsample all the predicted heatmaps with different resolutions to the resolution of the input image and average the heatmaps from all scales for final prediction. This strategy is quite different from previous methods [2, 22, 24] which only use heatmaps from a single scale or single stage for prediction.

The reason that we use heatmap aggregation is to enable scale-aware pose estimation. For example, the COCO Keypoint dataset [20] contains persons of large scale variance from 32^2 pixels to more than 128^2 pixels. Top-down methods [25, 8, 32] solve this problem by normalizing person regions approximately into a single scale. However, bottom-up methods need to be aware of scales to detect keypoints from all scales. We find heatmaps from different scales in HigherHRNet capture keypoints with different scales better. Thus, averaging predicted heatmaps from different resolutions makes HigherHRNet a scale-aware pose estimator.

To make our method as efficient as possible, we do not perform any multi-scale test during inference. Experimental results show that even without multi-scale test, our HigherHRNet outperforms the current best bottom-up methods with multi-scale test by a large margin. It shows that a simple solution has the potential to do well in multi-person pose estimation.

Method	Backbone	Input size	#Params	GFLOPs	AP	AP ⁵⁰	AP ⁷⁵	AP ^M	AP ^L
w/o multi-scale test									
OpenPose* [2]	—	—	—	—	61.8	84.9	67.5	57.1	68.2
Hourglass [22]	Hourglass	512	277.8M	206.9	56.6	81.8	61.8	49.8	67.0
PersonLab [24]	ResNet-101	1401	68.7M	405.5	66.5	88.0	72.6	62.4	72.3
Bottom-up HRNet [†]	HRNet-w32	512	28.5M	38.9	64.1	86.3	70.4	57.4	73.9
Ours	HRNet-w32	512	28.6M	44.6	66.4	87.5	72.8	61.2	74.2
Ours	HRNet-w48	640	63.8M	154.3	68.4	88.2	75.1	64.4	74.2
w/ multi-scale test									
Hourglass [22]	Hourglass	512	277.8M	206.9	63.0	85.7	68.9	58.0	70.4
Hourglass* [22]	Hourglass	512	277.8M	206.9	65.5	86.8	72.3	60.6	72.6
PersonLab [24]	ResNet-101	1401	68.7M	405.5	68.7	89.0	75.4	64.1	75.5
Ours	HRNet-w48	640	63.8M	154.3	70.5	89.3	77.2	66.6	75.8

* Indicates using refinement.

[†] Our implementation, not reported in [29]

Table 1. Comparisons with bottom-up methods on the COCO2017 test-dev set. All GFLOPs are calculated at single-scale. For PersonLab [24], we only calculate its backbone’s #Params and GFLOPs. Top: w/o multi-scale test. Bottom: w/ multi-scale test. *It is worth noting that our results are achieved without refinement.*

Method	AP	AP ⁵⁰	AP ⁷⁵	AP ^M	AP ^L	AR
Top-down methods						
Mask-RCNN [11]	63.1	87.3	68.7	57.8	71.4	—
G-RMI [25]	64.9	85.5	71.3	62.3	70.0	69.7
Integral Pose Regression [30]	67.8	88.2	74.8	63.9	74.0	—
G-RMI + extra data [25]	68.5	87.1	75.5	65.8	73.3	73.3
CPN [8]	72.1	91.4	80.0	68.7	77.2	78.5
RMPE [10]	72.3	89.2	79.1	68.0	78.6	—
CFN [13]	72.6	86.1	69.7	78.3	64.1	—
CPN (ensemble) [8]	73.0	91.7	80.9	69.5	78.1	79.0
SimpleBaseline [32]	73.7	91.9	81.1	70.3	80.0	79.0
HRNet-W48 [29]	75.5	92.5	83.3	71.9	81.5	80.5
HRNet-W48 + extra data [29]	77.0	92.7	84.5	73.4	83.1	82.0
Bottom-up methods						
OpenPose* [2]	61.8	84.9	67.5	57.1	68.2	66.5
Hourglass+AE*+ [22]	65.5	86.8	72.3	60.6	72.6	70.2
PersonLab+ [24]	68.7	89.0	75.4	64.1	75.5	75.4
Ours: HigherHRNet-W48+AE+	70.5	89.3	77.2	66.6	75.8	74.9

Table 2. Comparisons with both top-down and bottom-up methods on COCO2017 test-dev dataset. * means using refinement. + means using multi-scale test.

4. Experiments

4.1. COCO Keypoint Detection

Dataset. The COCO dataset [20] contains over 200,000 images and 250,000 person instances labeled with 17 keypoints. COCO is divided into *train/val/test-dev* sets with 57k, 5k and 20k images respectively. All the experiments in this paper are trained only on the *train* set. We report results on the *val* set for ablation studies and compare with other state-of-the-art methods on the *test-dev* set.

Evaluation metric. The standard evaluation metric is based on Object Keypoint Similarity (OKS): $OKS = \frac{\sum_i \exp(-d_i^2 / 2s^2 k_i^2) \delta(v_i > 0)}{\sum_i \delta(v_i > 0)}$. Here d_i is the Euclidean distance between a detected keypoint and its corresponding ground truth, v_i is the visibility flag of the ground truth, s is the object scale, and k_i is a per-keypoint constant that con-

Method	Feat. stride/resolution	AP	AP ^M	AP ^L
HRNet	4/128	64.4	57.1	75.6
HigherHRNet	2/256	66.9	61.0	75.7
HigherHRNet	1/512	66.5	61.1	74.9

Table 3. Ablation study of HRNet vs. HigherHRNet on COCO2017 val dataset. Using one deconvolution module for HigherHRNet performs best on the COCO dataset.

trols falloff. We report standard average precision and recall scores¹: AP⁵⁰ (AP at OKS = 0.50), AP⁷⁵, AP (the mean of AP scores at OKS = 0.50, 0.55, ..., 0.90, 0.95), AP^M for medium objects, AP^L for large objects, and AR (the mean of recalls at OKS = 0.50, 0.55, ..., 0.90, 0.95).

Training. Following [22], we use data augmentation with random rotation ([−30°, 30°]), random scale ([0.75, 1.25]), random translation ([−40, 40]) to crop an input image patch of size 512 × 512 as well as random flip. As mentioned in Section 3.4, we generate two ground truth heatmaps with resolutions 128 × 128 and 256 × 256 respectively.

We use the Adam optimizer [16]. The base learning rate is set to 1e−3, and dropped to 1e−4 and 1e−5 at the 200th and 260th epochs respectively. We train the model for a total of 300 epochs. To balance the heatmap loss and the grouping loss, we set the weight to 1 and 1e−3 respectively for the two losses.

Testing. We first resize the short side of the input image to 512 and keep the aspect ratio. Heatmap aggregation is done by resizing all the predicted heatmaps to the size of input image and taking the average. Following [22], flip testing is used for all the experiments. All reported numbers have been obtained with single model without ensembling.

¹<http://cocodataset.org/#keypoints-eval>

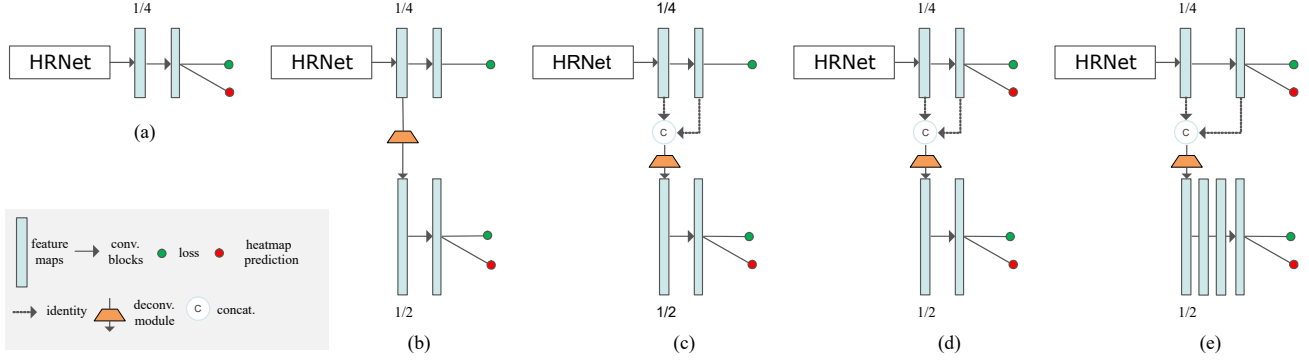


Figure 3. (a) Baseline method using HRNet [29] as backbone. (b) HigherHRNet with multi-resolution supervision (MRS). (c) HigherHRNet with MRS and feature concatenation. (d) HigherHRNet with MRS and feature concatenation. (e) HigherHRNet with MRS, feature concatenation and extra residual blocks. For (d) and (e), heatmap aggregation is used.

	Network	w/ MRS	feature concat.	w/ heatmap aggregation	extra res. blocks	AP	AP ^M	AP ^L
(a)	HRNet					64.4	57.1	75.6
(b)	HigherHRNet	✓				66.0	60.7	74.2
(c)	HigherHRNet	✓	✓			66.3	60.8	74.0
(d)	HigherHRNet	✓	✓	✓		66.9	61.0	75.7
(e)	HigherHRNet	✓	✓	✓	✓	67.1	61.5	76.1

Table 4. Ablation study of HigherHRNet’s components. MSR: multi-resolution supervision. feature concat.: feature concatenation. res. blocks: residual blocks.

Results on COCO2017 test-dev. Table 1 summarizes the results on COCO2017 test-dev dataset. From the results, we can see that using HRNet [29] itself already serves as a simple and strong baseline for bottom-up methods (64.1 AP). Our baseline method of HRNet with only single scale test outperforms Hourglass [22] using multi-scale test, while HRNet has much less parameters and computation in terms of FLOPs. Equipped with light-weight deconvolution modules, our proposed HigherHRNet (66.4 AP) outperforms HRNet by +2.3 AP with only marginal increase in parameters (+0.1M) and FLOPs (+14.7%). HigherHRNet is comparable with PersonLab [24] but with only 50% parameters and 11% FLOPs. If we further add refinement following [2, 22] with single pose estimator of HRNet [29], our HigherHRNet achieves 70.4 AP, outperforming all existing bottom-up methods by a large margin. We intend not to use multi-scale test because we want to keep our method as efficient as possible. The extra computation introduced by multi-scale test is usually much larger than using refinement.

Table 2 lists both bottom-up and top-down methods on the COCO2017 test-dev dataset. HigherHRNet further closes the performance gap between bottom-up and top-down methods.

4.2. Ablation Experiments

We perform a number of ablation experiments to analyze Higher-Resolution Network (HigherHRNet) on the

COCO2017 [20] val dataset.

HRNet vs. HigherHRNet. We perform ablation study comparing HRNet and HigherHRNet. For HigherHRNet, deconvolution module without extra residual blocks is used, and heatmaps aggregation is used for inference. Results are shown in Table 3. A simple bottom-up baseline by using HRNet with a feature stride of 4 achieves $AP = 64.4$. By adding one deconvolution module, our HigherHRNet with a feature stride of 2 outperforms HRNet by a large margin of +2.5 AP (achieving 66.9 AP). Furthermore, the main improvement comes from medium persons, where AP^M is improved from 57.1 for HRNet to 61.0 for HigherHRNet.

These results show that HigherHRNet performs much better with small scales thanks to its higher resolution heatmaps. We also find the AP for large person pose does no drop. This is mainly because we also use smaller resolution heatmaps for prediction. It demonstrates that 1) making prediction at higher resolution is beneficial to bottom-up pose estimation and 2) scale-aware prediction is important.

If we add a sequence of two deconvolution modules after HRNet to generate feature maps that is of the same resolution as the input image, we observe that the performance decreases to 66.5 AP from 66.9 AP for adding only one deconvolution module. The improvement for medium person is marginal (+0.1 AP) but there is a large drop in the performance of large person (−0.8 AP). We hypothesize this is because the misalignment between feature map scale and

object scales. Larger resolution feature maps (feature stride = 1) are good for detecting keypoints from even smaller persons but the small persons in COCO are not considered for pose estimation. Therefore, we only use one deconvolution module by default for the COCO dataset. But we would like to point out that the number of cascaded deconvolution modules should be dependent on datasets and we will validate this on more datasets in our future work.

HigherHRNet gain breakdown. To better understand the gain of the proposed components, we perform detailed ablation studies on each individual component. Figure 3 illustrates all the architectures of our experiments. Results are shown in Table 4.

Effect of deconvolution module. We perform ablation study on the effect of adding deconvolution module to generate higher resolution heatmaps. For a fair comparison, we only use the highest resolution feature maps to generate heatmaps for prediction (Figure 3 (b)). HRNet (Figure 3 (a)) achieves a baseline of 64.4 AP. By adding one deconvolution module, the model achieves 66.0 AP which is 1.6 AP better than the baseline. This improvement is completely due to predicting on larger feature maps with higher quality. The result verifies our claim that it is important to predict on higher resolution feature maps for bottom-up pose estimation.

Effect of feature concatenation. We concatenate feature maps with predicted heatmaps from HRNet as input to the deconvolution module (Figure 3 (c)) and the performance is further improved to 66.3 AP. We also observe there is a large gain in medium persons while the performance for large persons decreases. Comparing method (a) and (c), the gain of predicting heatmaps at higher resolution mainly comes from medium persons (+3.7AP^M). Moreover, the drop in large persons (−1.6 AP) justifies our claim that different different resolutions of feature maps are sensitive to different scales of persons.

Effect of heatmap aggregation. We further use all resolutions of heatmaps following the heatmap aggregation strategy for inference (Figure 3 (d)). Compared with Figure 3 (c) (66.3 AP) that only uses the highest resolution heatmaps for inference, applying heatmap aggregation strategy achieves 66.9 AP. Comparing method (d) and (e), the gain of heatmap aggregation comes from large person (+1.7 AP). And the performance of large person is even marginally better than predicting at lower resolution (method (a)). It means that predicting heatmaps using heatmap aggregation strategy is truly scale-aware.

Effect of extra residual blocks. We add 4 residual blocks in the deconvolution module and our best model achieves 67.1 AP. Adding residual blocks can further refine the feature maps and it increases AP for both medium and large persons equally.

Network	Input Size	GFLOPs	AP
HRNet	256	9.7	43.5
HRNet	384	21.9	57.0
HRNet	512	38.9	64.4
HRNet	640	60.8	65.4
HRNet	768	87.5	63.3
HRNet	896	119.1	58.8
HRNet	1024	155.6	54.3
HigherHRNet	256	11.2	52.3 _{↑7.8}
HigherHRNet	384	25.1	63.4 _{↑6.4}
HigherHRNet	512	44.6	67.1 _{↑2.7}
HigherHRNet	640	69.7	67.4 _{↑2.0}
HigherHRNet	768	100.4	64.7 _{↑1.3}
HigherHRNet	896	136.6	61.0 _{↑1.2}
HigherHRNet	1024	178.4	55.9 _{↑1.6}

Table 5. Ablation study of HigherHRNet with different input image size.

Training size	AP	AP ^M	AP ^L
512	67.1	61.5	76.1
640	68.5	64.3	75.3
768	68.5	64.9	73.8

Table 6. Ablation study of HigherHRNet with different training image size.

Input image size. Effects of input image size are shown in Table 5. As input size decreases, the gap between HRNet and HigherHRNet becomes larger, which means our HigherHRNet is much less affected by the resolution decreasing. It shows that for pose estimation on low-resolution image, generating higher resolution feature maps is the key to achieving good performance. HigherHRNet is thus a favorable choice when computational complexity is crucial and a small input resolution is demanded. For example, our HigherHRNet with input size of 384 has comparable performance to HRNet with input size of 512, however 13.8 GFLOPs (relative 36%) is saved.

Training with larger image size. In Table 5 we find HigherHRNet trained with input size 512 has the best evaluation performance with 640 test image size. A natural question is can training with larger input size further improve performance? To answer this question, we train HigherHRNet with 640×640 and 768×768 and results are shown in Table 6, all three models are tested using the training image size. We find that by increasing training image size to 640, there is a significant gain of 1.4 AP. Most of the gain comes from medium person while the performance of large person degrades slightly. When we further change the training image size to 768, the overall AP does not change anymore. We observe a marginal improvement in medium person along with large degradation in large person.

Backbone	#Params	GFLOPs	AP	AP ^M	AP ^L
HRNet-W32	28.6	47.8	68.5	64.3	75.3
HRNet-W40	44.5	110.7	69.2	64.9	75.9
HRNet-W48	63.8	154.3	69.9	65.4	76.4

Table 7. Ablation study of HigherRNet with different training image size.

Larger backbone. In previous experiments, we use HRNet-W32 (1/4 resolution feature map has 32 channels) as backbone. We perform experiments with larger backbones HRNet-W40 and HRNet-W48. Results are shown in Table 7. We find using larger backbone consistently improves performance for both medium and large person.

5. Conclusion

We have presented a Higher Resolution Network (HigherHRNet) which demonstrates the state-of-the-art performance for bottom-up multi-person human pose estimation. We find multi-scale image pyramid and larger input size can produce more accurate heatmaps for pose estimation but these methods suffer from high computational cost. Our proposed HigherHRNet is capable of efficiently generating multi- and higher-resolution heatmaps for more accurate human pose estimation. HigherHRNet outperforms all existing bottom-up methods by a large margin even without multi-scale test or large input size. In our future work, we will further study the scale problem in bottom-up multi-person human pose estimation and fully utilize feature pyramid.

Acknowledgments

Bowen Cheng and Thomas S. Huang are in part supported by IBM-ILLINOIS Center for Cognitive Computing Systems Research (C3SR) - a research collaboration as part of the IBM AI Horizons Network.

References

- [1] Vijay Badrinarayanan, Alex Kendall, and Roberto Cipolla. Segnet: A deep convolutional encoder-decoder architecture for image segmentation. *IEEE TPAMI*. 2
- [2] Zhe Cao, Tomas Simon, Shih-En Wei, and Yaser Sheikh. Realtime multi-person 2d pose estimation using part affinity fields. In *CVPR*, 2017. 1, 2, 4, 5, 6
- [3] Liang-Chieh Chen, Maxwell D. Collins, Yukun Zhu, George Papandreou, Barret Zoph, Florian Schroff, Hartwig Adam, and Jonathon Shlens. Searching for efficient multi-scale architectures for dense image prediction. In *NIPS*, 2018. 2
- [4] Liang-Chieh Chen, George Papandreou, Iasonas Kokkinos, Kevin Murphy, and Alan L Yuille. Deeplab: Semantic image segmentation with deep convolutional nets, atrous convolution, and fully connected crfs. *IEEE TPAMI*. 2
- [5] Liang-Chieh Chen, George Papandreou, Iasonas Kokkinos, Kevin Murphy, and Alan L Yuille. Semantic image segmentation with deep convolutional nets and fully connected crfs. 2015. 2
- [6] Liang-Chieh Chen, George Papandreou, Florian Schroff, and Hartwig Adam. Rethinking atrous convolution for semantic image segmentation. *arXiv preprint arXiv:1706.05587*, 2017. 2
- [7] Liang-Chieh Chen, Yukun Zhu, George Papandreou, Florian Schroff, and Hartwig Adam. Encoder-decoder with atrous separable convolution for semantic image segmentation. In *ECCV*, 2018. 2
- [8] Yilun Chen, Zhicheng Wang, Yuxiang Peng, Zhiqiang Zhang, Gang Yu, and Jian Sun. Cascaded pyramid network for multi-person pose estimation. In *CVPR*, 2018. 1, 2, 4, 5
- [9] Bowen Cheng, Yunchao Wei, Honghui Shi, Rogerio Feris, Jinjun Xiong, and Thomas Huang. Revisiting rcnn: On awakening the classification power of faster rcnn. In *ECCV*, 2018. 2
- [10] Hao-Shu Fang, Shuqin Xie, Yu-Wing Tai, and Cewu Lu. Rmpe: Regional multi-person pose estimation. In *ICCV*, 2017. 2, 5
- [11] Kaiming He, Georgia Gkioxari, Piotr Dollár, and Ross Girshick. Mask r-cnn. In *ICCV*, 2017. 1, 2, 5
- [12] Kaiming He, Xiangyu Zhang, Shaoqing Ren, and Jian Sun. Deep residual learning for image recognition. In *CVPR*, 2016. 2, 4
- [13] Shaoli Huang, Mingming Gong, and Dacheng Tao. A coarse-fine network for keypoint localization. In *ICCV*, 2017. 2, 5
- [14] Eldar Insafutdinov, Leonid Pishchulin, Bjoern Andres, Mykhaylo Andriluka, and Bernt Schiele. Deeppicut: A deeper, stronger, and faster multi-person pose estimation model. In *ECCV*, 2016. 2
- [15] Umar Iqbal and Juergen Gall. Multi-person pose estimation with local joint-to-person associations. In *ECCV*, 2016. 2
- [16] Diederik P Kingma and Jimmy Ba. Adam: A method for stochastic optimization. *arXiv preprint arXiv:1412.6980*, 2014. 5
- [17] Hei Law and Jia Deng. Cornernet: Detecting objects as paired keypoints. In *ECCV*, 2018. 4
- [18] Guosheng Lin, Anton Milan, Chunhua Shen, and Ian Reid. Refinenet: Multi-path refinement networks for high-resolution semantic segmentation. In *CVPR*, 2017. 2
- [19] Tsung-Yi Lin, Piotr Dollár, Ross Girshick, Kaiming He, Bharath Hariharan, and Serge Belongie. Feature pyramid networks for object detection. In *CVPR*, 2017. 2
- [20] Tsung-Yi Lin, Michael Maire, Serge Belongie, James Hays, Pietro Perona, Deva Ramanan, Piotr Dollár, and C Lawrence Zitnick. Microsoft coco: Common objects in context. In *ECCV*, 2014. 2, 4, 5, 6
- [21] Chenxi Liu, Liang-Chieh Chen, Florian Schroff, Hartwig Adam, Wei Hua, Alan Yuille, and Li Fei-Fei. Auto-deeplab: Hierarchical neural architecture search for semantic image segmentation. In *CVPR*, 2019. 2
- [22] Alejandro Newell, Zhiao Huang, and Jia Deng. Associative embedding: End-to-end learning for joint detection and

- grouping. In I. Guyon, U. V. Luxburg, S. Bengio, H. Wallach, R. Fergus, S. Vishwanathan, and R. Garnett, editors, *NIPS*. 2017. [1](#), [2](#), [3](#), [4](#), [5](#), [6](#)
- [23] Alejandro Newell, Kaiyu Yang, and Jia Deng. Stacked hourglass networks for human pose estimation. In *ECCV*, 2016. [2](#)
- [24] George Papandreou, Tyler Zhu, Liang chieh Chen, Spyros Gidaris, Jonathan Tompson, and Kevin Murphy. Personlab: Person pose estimation and instance segmentation with a part-based geometric embedding model. In *ECCV*, 2018. [1](#), [2](#), [4](#), [5](#), [6](#)
- [25] George Papandreou, Tyler Zhu, Nori Kanazawa, Alexander Toshev, Jonathan Tompson, Chris Bregler, and Kevin Murphy. Towards accurate multi-person pose estimation in the wild. In *CVPR*, 2017. [1](#), [2](#), [4](#), [5](#)
- [26] Leonid Pishchulin, Eldar Insafutdinov, Siyu Tang, Bjoern Andres, Mykhaylo Andriluka, Peter V Gehler, and Bernt Schiele. Deepcut: Joint subset partition and labeling for multi person pose estimation. In *CVPR*, 2016. [2](#)
- [27] Shaoqing Ren, Kaiming He, Ross Girshick, and Jian Sun. Faster r-cnn: Towards real-time object detection with region proposal networks. In *NIPS*, 2015. [2](#)
- [28] Olaf Ronneberger, Philipp Fischer, and Thomas Brox. U-net: Convolutional networks for biomedical image segmentation. In *MICCAI*. Springer. [2](#)
- [29] Ke Sun, Bin Xiao, Dong Liu, and Jingdong Wang. Deep high-resolution representation learning for human pose estimation. In *CVPR*, 2019. [1](#), [2](#), [3](#), [5](#), [6](#)
- [30] Xiao Sun, Bin Xiao, Fangyin Wei, Shuang Liang, and Yichen Wei. Integral human pose regression. In *Proceedings of the European Conference on Computer Vision (ECCV)*, pages 529–545, 2018. [1](#), [5](#)
- [31] Zbigniew Wojna, Vittorio Ferrari, Sergio Guadarrama, Nathan Silberman, Liang-Chieh Chen, Alireza Fathi, and Jasper Uijlings. The devil is in the decoder. In *BMVC*, 2017. [2](#)
- [32] Bin Xiao, Haiping Wu, and Yichen Wei. Simple baselines for human pose estimation and tracking. In *ECCV*, 2018. [1](#), [2](#), [4](#), [5](#)
- [33] Tien-Ju Yang, Maxwell D Collins, Yukun Zhu, Jyh-Jing Hwang, Ting Liu, Xiao Zhang, Vivienne Sze, George Papandreou, and Liang-Chieh Chen. Deeperlab: Single-shot image parser. *arXiv preprint arXiv:1902.05093*, 2019. [2](#)
- [34] Fisher Yu and Vladlen Koltun. Multi-scale context aggregation by dilated convolutions. *arXiv preprint arXiv:1511.07122*, 2015. [2](#)